ADVANCED OPTICAL MATERIALS
www.advopticalmat.de

On-Chip Mercury-Free Deep-UV Light-Emitting Sources with Ultrahigh Germicidal Efficiency

Vijay Kumar Sharma, Swee Tiam Tan, Zheng Haiyang, Sushant Shendre, Alexandra Baum, Francis Chalvet, Jonas Tirén, and Hilmi Volkan Demir**

In the current COVID-19 scenario, there is an urgent need for developing efficient and mercury-free deep-ultraviolet (deep-UV) light sources for disinfection applications. AlGaN-based light-emitting diodes (LEDs) may be considered as an alternative, but due to their inherent low efficiencies in the deep-UV spectral region, significant developments are required to address efficiency issues. Here, a mercury-free chip-size deep-UV light source is shown which is enabled by high-vacuum chip-scale cavity sealing overcoming the limitations of both mercury lamps and deep-UV LEDs. These deep-UV chips are cathodoluminescence based, in which a cavity is created with high vacuum integrity for efficient field-emission. These chips demonstrate optical output power ≥20 mW (efficiency ≈4%) and, owing to the spectral overlap of phosphor cathodoluminescence spectra and germicidal effectiveness curve, resulted in log 6 (99.9999%) germicidal efficiency. Additionally, these chips offer high reliability, "instant" ON/OFF capability, high operational lifetimes, and low-temperature dependence with complete design freedom.

1. Introduction

Compact and highly efficient UVC (200–280 nm) light sources, especially the 250–280 nm wavelength range, are of considerable technological interest as an alternative to traditional mercury lamps for disinfection applications.[1–5] Mercury lamps are commonly used in the municipal water and waste-water purification, but for consumer and consumer near products (refrigerators, air conditioners, disinfection cabinets, etc.) there are significant limitations because of mercury toxicity. The world has also acknowledged the adverse effects of mercury on human health and the environment, leading to the Minamata Convention on mercury, signed by 128 countries to reduce global emissions of mercury.[6] This convention has already entered into force from August 2017 and will eventually phase out the use of mercury in existing products or processes, resulting in strong demand for alternative deep-ultraviolet (deep-UV) light sources. AlGaN-based UV light-emitting diodes (LEDs) are considered as excellent candidates to replace mercury lamps.[7] AlGaN-based LEDs can be tuned to cover almost the entire UV spectrum from 210 to 355 nm by alloying GaN with AlN materials.[8–11] However, the output power and emission efficiency of these deep-UV LEDs are limited because of several inherent issues including, i) high dislocation densities, ii) low hole concentrations, and iii) low light extraction efficiency for the AlGaN-based LEDs.[7,11] To date, the maximum power efficiency (PE, defined as P_{out}/P_{in}) reported for the state-of-art packaged deep-UV LEDs emitting at 265 nm (considered as the gold standard for disinfection) are below 1%, which is the main driving force to seek for other alternatives.[3]

Electron-beam (e-beam) pumped semiconductor-based light sources have also been explored as a promising alternative.[12] For example, Watanabe et al.[13] reported a device using hexagonal boron nitride powders emitting at a wavelength of 225 nm, with a maximum output power of 1 mW and power efficiency of 0.6%. Additionally, Shimahara et al.[14] demonstrated an output power of 2.2 mW at 247 nm with a power efficiency of 0.24% from e-beam excited silicon-doped AlGaN bulk-like film. To take it forward, Fukuyo et al.[15] optimized the silicon-doped AlGaN multiple quantum wells (MQWs)

Dr. V. K. Sharma, Dr. S. T. Tan, Dr. Z. Haiyang, Dr. S. Shendre, Prof. H. V. Demir
LUMINOUS! Center of Excellence for Semiconductor Lighting and Displays
School of Electrical and Electronic Engineering
School of Physical and Mathematical Sciences
Nanyang Technological University
Singapore 639798, Singapore
E-mail: hvdemir@ntu.edu.sg
Dr. V. K. Sharma, Prof. H. V. Demir
UNAM-National Nanotechnology Research Center and Institute of Materials Science and Nanotechnology
Department of Electrical and Electronics Engineering
Department of Physics
Bilkent University
Ankara 06800, Turkey
Prof. S. T. Tan
School of Energy and Chemical Engineering
Xiamen University Malaysia
Jalan Sunsuria, Bandar Sunsuria, Sepang, Selangor 43900, Malaysia
Dr. A. Baum, Dr. F. Chalvet, Dr. J. Tirén
LightLab Sweden AB
Uppsala Business Park
Virdings Allé 32B, Uppsala 754 50, Sweden
E-mail: JonasT@lightlab.se
The ORCID identification number(s) for the author(s) of this article can be found under https://doi.org/10.1002/adom.202100072.

DOI: 10.1002/adom.202100072

 © 2021 Wiley-VCH GmbH

and reported that e-beam excitation will result in the deep-UV light output power of 15 mW with a conversion efficiency of 0.75% at a wavelength of 256 nm. Using e-beam pumped AlGaN MQWs, similar levels of power efficiency were reported by Ivanov et al.[16] (≈0.24% at 270 nm), Rong et al.[11] (≈0.43% at 285 nm), Wang et al.[17] (≈0.75% at 267 nm), Tabataba-Vakili et al.[18] (≈0.43% at 246 nm), and Jmerik et al.[19] (≈0.75% at 235 nm). However, similar to deep-UV LEDs their performance levels are inadequate for practical applications.[1,20,21] Oto et al.[22] in a breakthrough demonstrated an output of 100 mW with a phenomenal power efficiency of ≈40% from e-beam pumped AlGaN/AlN MQWs emitting at ≈240 nm using a thermal-electron gun operated inside a vacuum chamber. Although the physical mechanisms resulting in this power efficiency were not fully understood, this work has highlighted the prospects of e-beam pumped deep-UV light sources. Recently, several researchers[23,24,25] started replacing the thermal electron gun with the cold field emitters owing to their compactness for practical applications. Matsumoto et al.[25] make a significant improvement in this direction by demonstrating a device having 20 mW power at 240 nm with the power efficiency of 4% obtained by combining AlGaN MQWs and graphene nanoneedle field electron emitters. Interestingly, in all the previous reports, there was no specific focus on the emission wavelength and except for ref. [25] the power efficiency in all cases is less than 1%. Also, most of the previous demonstration relies on using a thermal electron-gun, which requires a vacuum chamber, making it impractical for commercial applications.

In this work, overcoming the limitations of all existing technologies, we have developed a chip-size, efficient deep-UV light source based on a 100% mercury-free approach, enabled by on-chip cathodoluminescence and field-emission. Our deep-UV chips offer high reliability, "instant" ON/OFF capability, high operational lifetimes (500 h), low-temperature dependence (–20 to 80 °C), and complete design freedom. Besides, we have also demonstrated ultrahigh germicidal efficiency log 6 (99.9999%) using our deep-UV chips. We believe our chips being mercury-free and compact with high germicidal efficiency will be beneficial for many disinfection applications that require environmental-friendly solutions and the use of limited spaces.

2. Results and Discussion

Figure 1 shows our fabricated deep-UV chips with all material components. The chip is cathodoluminescence based, in which a high-integrity vacuum cavity is created allowing for efficient field-emission. In our deep-UV chips, we use high-quality ZnO nanorods as a cold cathode, where we apply a high voltage (but extremely low current, and thus very low electrical power) in operation. The electrical field at the tips of the nanorod arrays (NRs) is so strong that the electrons are drawn out of the material. The electrons are then accelerated in a vacuum by the applied electric field toward the anode, which is coated with UVC phosphor ($Lu_2Si_2O_7:Pr^{3+}$) that generates deep-UV light when hit by these electrons.

For the highly efficient and stable deep-UV light sources, it is important to fabricate a field electron emitter with stable emission even in the presence of a small amount of residual gases. Although carbon nanotubes have attracted much attention due to their low turn-on field and large emission current density,[26–28] several other nanostructures, such as ZnO nanowires,[29] SiC nanowires,[30] and AlN nanoneedles[31] were also considered potential options for field-emission. Especially ZnO nanostructures have been investigated extensively for field-emission for a long time. Compared to carbon-based materials, the ZnO nanostructures have a unique advantage: being an oxide material, the requirement for vacuum becomes less critical, i.e., ZnO field emitters would last longer compared to carbon-based field-emission device used in the same vacuum conditions.[32] Various previous studies reported field-emission of ZnO nanorods/nanowires at high current density, with low turn-on field, and highly stable emission.[33–36] Therefore, we selected ZnO nanorods as a convenient e-beam excitation source for the fabrication of our chip-sized deep-UV emission device. The other parameters taken into account were the low cost, and easy and robust synthesis technique to make it convenient for practical applications. In our case, ZnO nanorods were fabricated using controlled oxidation (O_2 mixed in N_2) of the brass mesh resulting in the average length of ≈10–15 µm and the diameter ≈150–200 nm. **Figure 2**a shows the cross-sectional scanning electron microscope (SEM) images of the ZnO nanorods used as field-emitters on the cathode side in the deep-UV chips. The inset of Figure 2a shows the top view of the ZnO

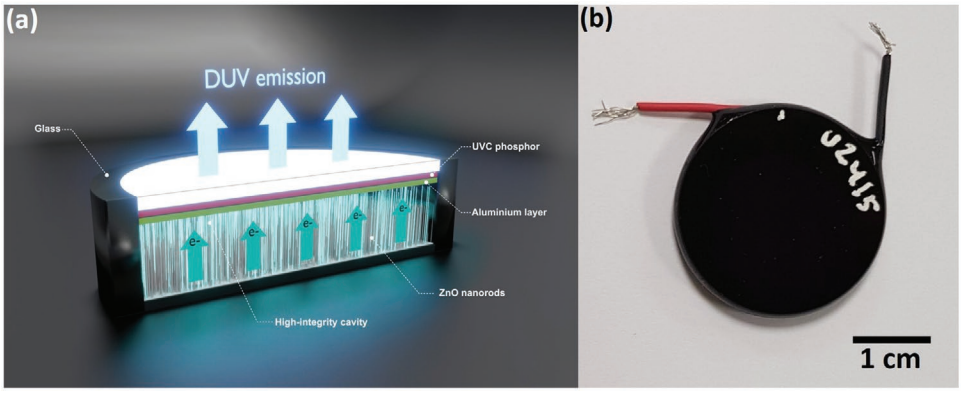

Figure 1. a) Our deep-UV device architecture. b) A prototype of our fabricated deep-UV chip.

© 2021 Wiley-VCH GmbH

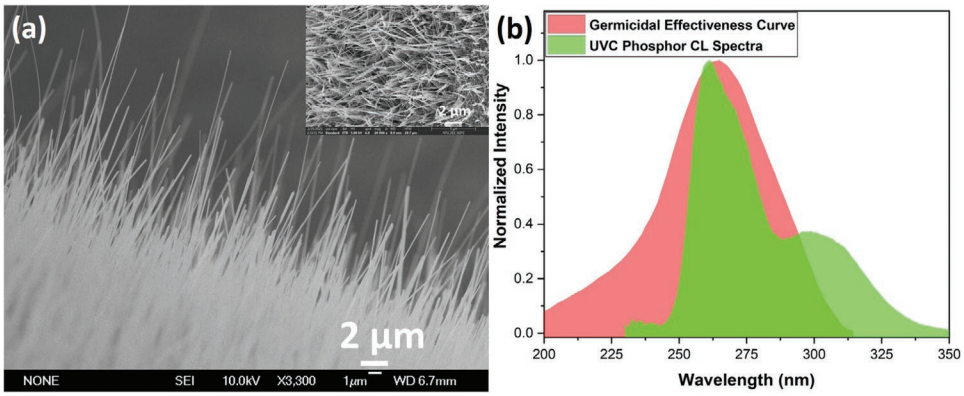

Figure 2. a) Cross-sectional and top-view (in the inset) of ZnO nanorods used as the cathode and b) cathodoluminescence spectra of the anode (UVC phosphor; $Lu_2Si_2O_7:Pr^{3+}$) used in our deep-UV chip and its overlap with germicidal effectiveness curve.

nanorods. Figure 2b shows the cathodoluminescence spectra of the UVC phosphor ($Lu_2Si_2O_7:Pr^{3+}$) used in our chips.

Figure 2b shows the overlap of the cathodoluminescence spectra of the UVC phosphor with the well-known germicidal effectiveness curve. We can see the germicidal effectiveness curve matches nicely with the cathodoluminescence spectra of the UVC phosphor with a spectral overlap of ≈65%. For a deep-UV light source to be powerful for disinfection applications, we must choose an efficient phosphor with a maximum overlap of its emission spectra with the germicidal effectiveness curve. This is the reason we specifically have chosen UVC phosphor having the wavelength maxima adjacent to 265 nm since this wavelength is lethal for pathogens and generally known as the gold standard for disinfection.[37] The films of UVC phosphor were screen-printed on UVC transparent glass substrates. A 60 nm thick aluminium layer was deposited on top of the UVC phosphor to serve multiple functions, i.e., i) conducting layer of the anode, ii) reflect the backscattered component of deep-UV emission forward, and iii) to reduce charging.

Figure 3a shows an image of our deep-UV chip in the operating state, which is composed of ZnO NRs cold cathode and $Lu_2Si_2O_7:Pr^{3+}$ UVC phosphor as an anode. The cathode and anode side of the deep-UV chips were placed inside a vacuum chamber where they were evacuated to reach a base pressure of 10^{-7} hPa, and then, sealed using glass paste at high temperatures (380–450 °C). The wired contacts were made after the sealed chips were taken out of the vacuum chamber and before the measurements, the chips were properly isolated using an epoxy. Deep-UV emission is observed immediately after the application of high voltage and was collected through the back of the UVC transparent glass substrate. The total deep-UV power through the UVC transparent substrate was measured using an ILT2400 handheld light meter (calibrated at 270 nm). The anode and cathode side were separated by 2 mm in our deep-UV chips. The full chip size after the insulation is 27 mm in diameter and 4 mm in thickness, which offers complete design freedom. Figure 3b shows the fluorescence (UV marks) on the 10 Dollar Singapore currency note obtained using UV light from our deep-UV chips. In our deep-UV chips, the upper bound on the efficiency is determined by the cathodoluminescence efficiency of the UVC phosphor used.[38] The cathodoluminescence efficiency of the UVC phosphor used in our deep-UV chips is ≈10%. In general, there are few other options for UVC phosphors/emitters but their cathodoluminescence efficiencies are mostly below 10% and also their emission spectrum is quite different from the germicidal effectiveness curve which makes them ineffective for disinfection applications.[12,39,40]

The field emission properties (current density–voltage (J–V)) of the deep-UV chips are plotted in **Figure 4**a. The current density–voltage characteristics exhibited an exponential-like

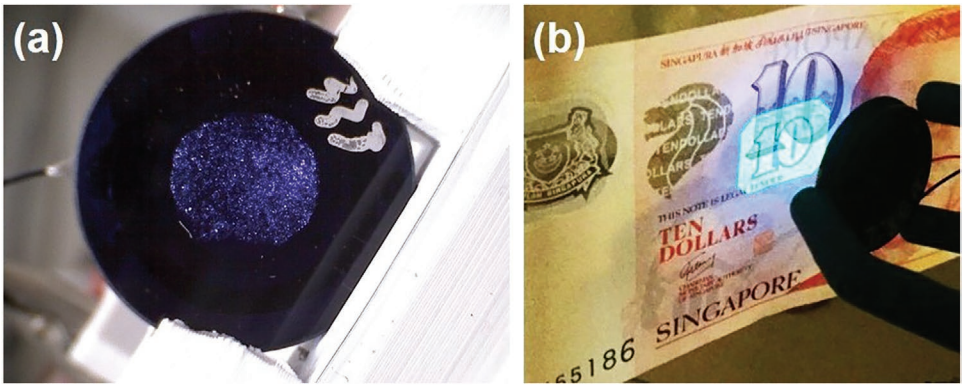

Figure 3. a) Chip in the operating state (only blue part is visible, which is only 0.4% of the total UV spectrum). b) UV marks on 10 Singapore dollars are visible with our deep-UV chips.

© 2021 Wiley-VCH GmbH

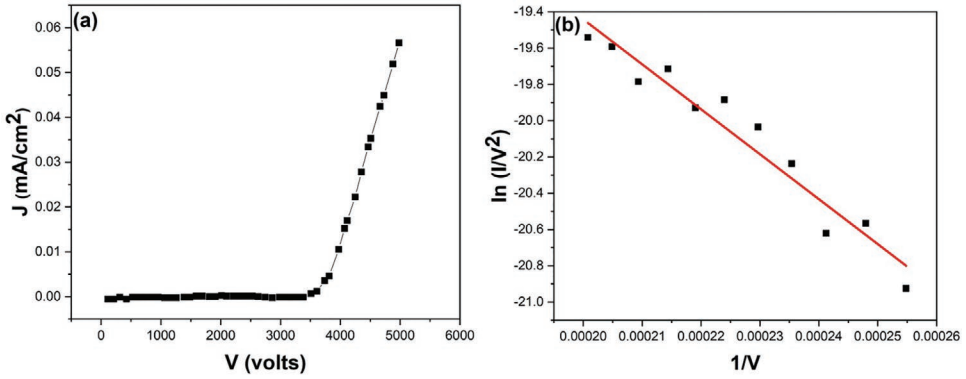

Figure 4. a) Current density–voltage (*J*–*V*) characteristics of our deep-UV chip and b) the corresponding Fowler–Nordheim plot.

behavior, which was found to be reproducible for all investigated chips. The Fowler–Nordheim plot for our deep-UV device is shown in Figure 4b. The variation of $\ln(I/V^2)$ with $(1/V)$ is a straight line, confirming that the current was indeed caused by electron field emission.

According to the Fowler–Nordheim electron emission theory,[41] the emission current density is described as

$$J = A\left(\frac{\beta^2 E^2}{\phi}\right)\exp\left(-B\phi^{\frac{3}{2}}/\beta E\right) \quad (1)$$

where $E = (V/d)$ is the applied field, d is a distance between the anode and the cathode, and V is the applied voltage, ϕ is the work function, which is 5.3 eV for ZnO, A and B are constants with the values of 1.56×10^{-10} AV^{-2} eV and 6.87×10^9 V $eV^{-3/2}$ m^{-1}, respectively, and β is a field enhancement factor. β represents the amplification of the electric field at the tip, compared to its macroscopic value. We can estimate the value of the field enhancement factor (β) from the Fowler–Nordheim plots. The slope of the F–N plot is equal to $B\phi^{\frac{3}{2}}d/\beta$, where d is the distance between ZnO nanorods and the anode. From the above equation, β is estimated to be 2270 for our ZnO nanorods, which is sufficient for various field-emission applications. In the literature, a large range of β values have been reported for various ZnO nanostructures, e.g., $\beta \approx 847$ (nanowires, Lee et al.[29]), $\beta \approx 657$ (nanopins, Xu and Sun[42]), $\beta \approx 570$ (nanotubes, Shen et al.[48]), $\beta \approx 6285$ (tetrapods, Wan et al.[43]), $\beta \approx 2300$ (NRs, Pan et al.[44]), and $\beta \approx 3010$ (nanowire arrays, Xu et al.[45]). Some previous works using cascaded two-stage field emitters reported very high values of β, e.g., $\beta \approx 10\,179$ (graphene on ZnO nanowires, Maiti et al.[34]) and $\beta \approx 6975$ (graphene attached to ZnO tetrapods, Maiti et al.[46]). The value of β is known to depend on the geometry, crystal structure, and density of ZnO nanostructures.[42,47] The moderately high value of β in our case is mainly because of the high aspect ratio and reasonably aligned arrays of ZnO NRs as can be seen from Figure 2a.

We obtained an average power ≥ 20 mW from our deep-UV chips for stable operation at an electrical input power of 500 mW (5.5–6.5 kV, 0.075–0.090 mA). We have also observed a maximum output of 30 mW, which shows the potential for further optimization. To the best of our knowledge, only Watanabe et al.[13] and Matsumoto et al.[25] fabricated portable battery-operated deep-UV emission device with smaller dimensions. Although Matsumoto et al.[25] obtained 20 mW power with power efficiency ≈4% in their case, the wavelength was not optimized to maximize the germicidal disinfection. Also, they did report any germicidal efficiency using their device. Whereas in the case of Watanabe et al.[13] the maximum power obtained was only 1 mW at the wavelength of 225 nm, which is too low for practical applications. In our deep-UV chips, we obtained an average power of 20 mW with a power efficiency of ≈4% at the 261 nm peak wavelength close to the germicidal wavelength. Also, in our case, the spectral overlap is ≈65% with the germicidal effectiveness curve allowing us to maximize the disinfection capabilities of our deep-UV chips. The average power and power efficiency obtained in our case at the germicidal wavelength is the highest among all the portable deep-UV light sources reported in the literature.

We have performed a rigorous lifetime test of our deep-UV chips, which is a mandatory requirement for practical applications. Our deep-UV chips have "instant" ON/OFF capabilities like LEDs, unlike mercury lamps which take few minutes to turn completely ON. This is crucial in applications where immediate disinfection is needed, e.g., when turning on a water tap. **Figure 5**a shows the optical output power of our deep-UV chips with the operating hours at a constant input power of 500 mW in 60 s ON/60 s OFF intermittent operation. We observed initial degradation in output deep-UV power but, after that, it is constant for up to 1000 h. We believe the initial decrease in output power is mainly caused by the degradation of phosphor surface by electron bombardment until a stable surface layer is reached. At the current stage, the lifetime of the majority of the tested deep-UV chips is ≈500 h and is expected to be higher after further optimizations.

Further, we have also tested the performance of the deep-UV chips at different operating temperature conditions as required by various home appliance applications, which are not possible by the traditional mercury lamps. The results show that our chips performance remains almost similar within the whole temperature range from −20 to 80 °C, whereas the mercury lamps perform best within the temperature range 35–55 °C, as shown in Figure 5b. Our deep-UV chips have also undergone and passed reliability testing including those for moisture, temperature cycling, vibration, and mechanical shock.

© 2021 Wiley-VCH GmbH

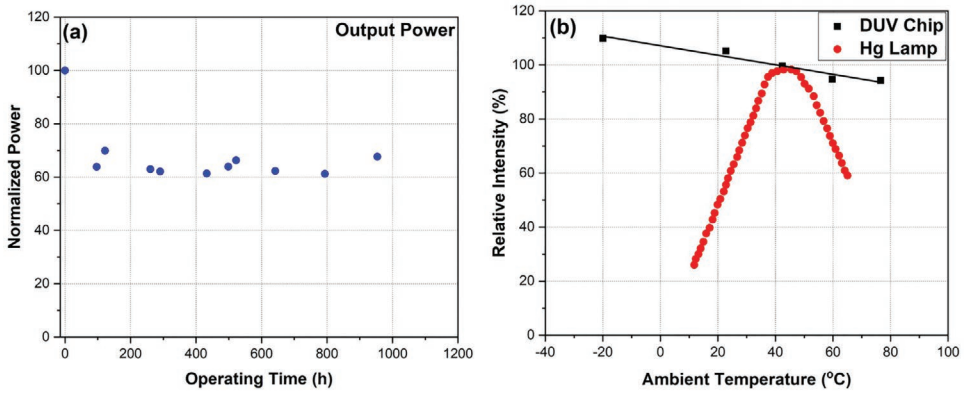

Figure 5. a) Variation of output power with time (lifetime test). b) Light source intensity (output power) dependence on different operating temperature conditions.

Additionally, our chips do not require any additional thermal management for operating at elevated temperatures as opposed to UVC LEDs where it is a mandatory requirement otherwise resulting in a substantial drop in efficiency.[49] Nevertheless, it is predicted that for UVC LEDs with 285 emission wavelength, wall-plug efficiency will exceed 10% mark by 2021.[3] But same is not true for UVC LEDs emitting at 265 nm which is considered as the gold standard for germicidal disinfection, whereas, in our case, we obtained 4% efficiency with our deep-UV chips emitting at 261 nm in the package similar to LEDs. Currently, we are working on enhancing efficiency and lifetime by further optimizing device design and by implementing light extraction techniques.

Lastly, we performed germicidal experiments to study the germicidal efficacy (disinfection capabilities) of our deep-UV chips. In our experiments, we use a single chip having an input power of 500 mW placed at 7.5 cm from the Petri dish containing *Escherichia coli* (*E. coli*) bacteria on tryptic soy agar. *E. coli* ATCC 8739 bacteria of known concentration, e.g., 1000, 10 000, 100 000, 1 000 000 colony-forming units, have been irradiated with our chip for 60, 120, 240, and 510 s. We also have a control sample, which is not irradiated by deep-UV light. After that, *E. coli* bacteria are incubated for 3 days at 30–35 °C. **Figure 6**a shows the photographs of *E. coli* bacteria after 24 h incubation on a nonirradiated and deep-UV irradiated sample, respectively. We found that after ≈47 mJ cm^{-2} (510 s) of deep-UV irradiation, we obtain log 6 (99.9999%) reduction in *E. coli* bacteria using our chip (see Figure 6b). In the literature, several different values have been reported due to the specific strains and the different irradiation conditions.[50] The disinfection time can be reduced greatly by using more deep-UV chips. Additionally, we also do not observe tailing in our chips, which is quite common in mercury lamps. We believe the reason for the absence of tailing with our deep-UV chips is the 65% match of the cathodoluminescence spectra of UVC phosphor with germicidal effectiveness curve and the presence of an additional 298 nm wavelength radiation. However, this speculation requires further investigations. It is also implied that pulsed UVC irradiation is more effective than the continuous irradiation from the mercury lamp in eradicating various pathogens.[50] Our chips having "instant" ON/OFF capability can be easily used in the pulsed mode offering cost-effective efficient disinfection. Recently, few groups evaluated and suggested that UVC irradiation is a suitable disinfection method for eradicating COVID-19 coronavirus.[51,52] We believe our deep-UV chips with high germicidal efficiency can help in containing the outbreak by disinfecting the commonly touched surfaces.

3. Conclusions

In summary, we have demonstrated efficient (≈4% efficiency) chip-size mercury-free deep-UV light sources with the power ≥ 20 mW. The tested lifetime of our deep-UV chip at this stage is 500 h and is expected to be higher after structural refinements and further optimization. Most importantly, the germicidal

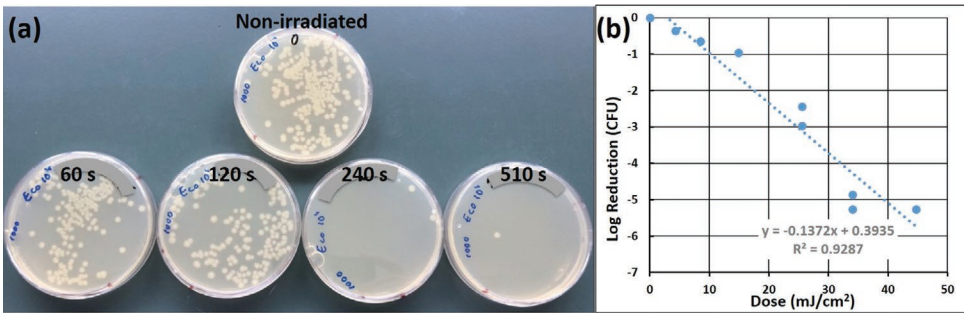

Figure 6. a) Petri dish containing *E. coli* bacteria before and after deep-UV irradiation from our chips (nonirradiated and radiated for 60, 120, 240, and 510 s). b) Log-reduction obtained from our deep-UV chips.

© 2021 Wiley-VCH GmbH

reduction obtained by our deep-UV chips is of the order of log 6, which is at par with the mercury lamps. Besides, our chips are economical (intermittent operation) and environmentally (mercury-free) friendly in comparison to mercury lamps. Our innovative deep-UV light chip technology with its exceptional germicidal performance, immediate start-up, low-temperature dependence, and small size is expected to open up new disinfection applications in consumer near products. The potential applications of the deep-UV chips include disinfection in home appliances and more importantly in hospitals and childcare centers to control the outbreak of infectious diseases by disinfecting contaminated surfaces.

4. Experimental Section

UVC phosphor ($Lu_2Si_2O_7$:Pr^{3+}) was custom developed by the company Leuchtstoffwerk Breitungen GmbH. The average particle size (D_{50}) of the UVC phosphor was ≈5–6 µm. A screen-printing process was used to deposit phosphor films on the UVC transparent glass substrates. The phosphor was covered with a sputtered aluminium thin film of 60 nm thickness, forming the deep-UV fluorescent screen. ZnO field emitters (NRs) were fabricated using controlled oxidation (O_2 mixed in N_2) of brass mesh at 550 °C in the tube furnace. The typical length of the ZnO NRs was in the range 10–15 µm and their diameter was between 150 and 200 nm, leading to a high aspect ratio of 70, which made them suitable as a field electron emission cathode. These parts were assembled in a vacuum chamber and sealed at the vacuum pressure of 10^{-7} hPa.

The high-voltage power supply was used to drive the deep-UV chips and the output light power was measured using two different detectors to check the consistency of the results. In this manuscript, the CL spectra were measured by a JETI specbos UV spectroradiometer (D = 10 cm) and the reported radiant flux was measured using an ILT2400 handheld light meter (D = 4 cm). Both detectors resulted in similar values within the ±10% range. An ILT2400 handheld light meter with a SED270-QT input optics (calibrated at 270 nm) measured irradiance in W cm^{-2} and was used for measuring power. On the other hand, JETI specbos 1211UV spectroradiometer with a diffuser was used to measure spectral radiance Ee in W $(m^2*nm)^{-1}$. The irradiance E in W cm^{-2} was calculated by integrating Ee over the spectrum. The total radiant flux Φ in W was calculated by the following equation, assuming a circular Lambertian source and the validity of the inverse square law

$$\Phi = ED^2\pi \tag{2}$$

with D being the distance of light source and detector.

Acknowledgements

This research project entitled "Next-Generation Ultralow-Cost High-Efficiency Eco-Friendly Lamps" is jointly supported by LightLab AB, Sweden and NTU, Singapore.

Conflict of Interest

The authors declare no conflict of interest.

Author Contributions

H.V.D. and J.T. conceived the idea and supervised the work at all stages. V.K.S. and S.T.T. led this work from Nanyang Technological University (NTU), Singapore whereas A.B. and F.C. led this work from LightLab AB, Sweden. Z.H. and S.S. helped with the measurement's setup, screen printing, and sputtering experiments. The manuscript is a combined effort of all the authors.

Data Availability Statement

The data that support the findings of this study are available from the corresponding author upon reasonable request.

Keywords

cathodoluminescence, deep-ultraviolet chips, disinfection applications, ultrahigh germicidal efficiency, UVC light sources

Received: January 12, 2021
Revised: March 14, 2021
Published online: May 6, 2021

[1] A. Khan, K. Balakrishnan, T. Katona, A. Khan, *Nat. Photonics* **2008**, *2*, 77.
[2] M. S. Shur, R. Gaska, *IEEE Trans. Electron Devices* **2010**, *57*, 12.
[3] M. Kneissl, T. Y. Seong, J. Han, H. Amano, *Nat. Photonics* **2019**, *13*, 233.
[4] Shining a light on COVID-19, *Nat. Photonics* **2020**, *14*, 337.
[5] D. Li, K. Jiang, X. Sun, C. Guo, *Adv. Opt. Photonics* **2018**, *10*, 43.
[6] United Nations Environment Programme, **2017**.
[7] H. Hirayama, N. Maeda, S. Fujikawa, S. Toyoda, N. Kamata, *Jpn. J. Appl. Phys.* **2014**, *53*, 100209.
[8] C. Pernot, S. Fukahori, T. Inazu, T. Fujita, M. Kim, Y. Nagasawa, A. Hirano, M. Ippommatsu, M. Iwaya, S. Kamiyama, I. Akasaki, H. Amano, *Phys. Status Solidi A* **2011**, *208*, 1594.
[9] V. N. Jmerik, A. M. Mizerov, A. A. Sitnikova, P. S. Kop'ev, S. V. Ivanov, E. V. Lutsenko, N. P. Tarasuk, N. V. Rzheutskii, G. P. Yablonskii, *Appl. Phys. Lett.* **2010**, *96*, 141112.
[10] H. Yoshida, Y. Yamashita, M. Kuwabara, H. Kan, *Nat. Photonics* **2008**, *2*, 551.
[11] X. Rong, X. Wang, S. V. Ivanov, X. Jiang, G. Chen, P. Wang, W. Wang, C. He, T. Wang, T. Schulz, M. Albrecht, V. N. Jmerik, A. A. Toropov, V. V. Ratnikov, V. I. Kozlovsky, V. P. Martovitsky, P. Jin, F. Xu, X. Yang, Z. Qin, W. Ge, J. Shi, B. Shen, *Adv. Mater.* **2016**, *28*, 7978.
[12] E. F. Schubert, J. Cho, *Nat. Photonics* **2010**, *4*, 735.
[13] K. Watanabe, T. Taniguchi, T. Niiyama, K. Miya, M. Taniguchi, *Nat. Photonics* **2009**, *3*, 591.
[14] Y. Shimahara, H. Miyake, K. Hiramatsu, F. Fukuyo, T. Okada, H. Takaoka, H. Yoshida, *Appl. Phys. Express* **2011**, *4*, 042103.
[15] F. Fukuyo, S. Ochiai, H. Miyake, K. Hiramatsu, H. Yoshida, Y. Kobayashi, *Jpn. J. Appl. Phys.* **2013**, *52*, 01AF03.
[16] S. V. Ivanov, V. N. Jmerik, D. V. Nechaev, V. I. Kozlovsky, M. D. Tiberi, *Phys. Status Solidi A* **2015**, *212*, 1011.
[17] Y. Wang, X. Rong, S. Ivanov, V. Jmerik, Z. Chen, H. Wang, T. Wang, P. Wang, P. Jin, Y. Chen, V. Kozlovsky, D. Sviridov, M. Zverev, E. Zhdanova, N. Gamov, V. Studenov, H. Miyake, H. Li, S. Guo, X. Yang, F. Xu, T. Yu, Z. Qin, W. Ge, B. Shen, X. Wang, *Adv. Opt. Mater.* **2019**, *7*, 1801763.
[18] F. Tabataba-Vakili, T. Wunderer, M. Kneissl, Z. Yang, M. Teepe, M. Batres, M. Feneberg, B. Vancil, N. M. Johnson, *Appl. Phys. Lett.* **2016**, *109*, 181105.

© 2021 Wiley-VCH GmbH

[19] V. N. Jmerik, D. V. Nechaev, A. A. Toropov, E. A. Evropeitsev, V. I. Kozlovsky, V. P. Martovitsky, S. Rouvimov, S. V. Ivanov, *Appl. Phys. Express* **2018**, *11*, 091003.
[20] H. Hirayama, Y. Tsukada, T. Maeda, N. Kamata, *Appl. Phys. Express* **2010**, *3*, 031002.
[21] H. Hirayama, S. Fujikawa, N. Noguchi, J. Norimatsu, T. Takano, K. Tsubaki, N. Kamata, *Phys. Status Solidi A* **2009**, *206*, 1176.
[22] T. Oto, R. G. Banal, K. Kataoka, M. Funato, Y. Kawakami, *Nat. Photonics* **2010**, *4*, 767.
[23] S. T. Yoo, B. So, H. I. Lee, O. Nam, K. C. Park, *AIP Adv.* **2019**, *9*, 075104.
[24] W. Z. Tawfik, C. M. M. Kumar, J. Park, S. K. Shim, H. Lee, J. Lee, J. H. Han, S.-W. Ryu, N. Lee, J. K. Lee, *J. Mater. Chem. C* **2019**, *7*, 11540.
[25] T. Matsumoto, S. Iwayama, T. Saito, Y. Kawakami, H. Amano, F. Kubo, H. Amano, *Opt. Express* **2012**, *20*, 24320.
[26] J. T. L. Thong, C. H. Oon, W. K. Eng, W. D. Zhang, L. M. Gan, *Appl. Phys. Lett.* **2001**, *79*, 2811.
[27] Q. Liao, Y. Zhang, Y. Huang, J. Qi, Z. Gao, L. Xia, H. Zhang, *Appl. Phys. Lett.* **2007**, *90*, 151504.
[28] S. T. Yoo, J. H. Hong, J. S. Kang, K. C. Park, *J. Vac. Sci. Technol., B* **2018**, *36*, 02C103.
[29] C. J. Lee, T. J. Lee, S. C. Lyu, Y. Zhang, H. Ruh, H. J. Lee, *Appl. Phys. Lett.* **2002**, *81*, 3648.
[30] C. S. L., S. T. L. K. W. Wong, X. T. Zhou, F. C. K. Au, H. L. Lai, *Appl. Phys. Lett.* **1999**, *75*, 2918.
[31] Y. B. Tang, H. T. Cong, Z. M. Wang, H.-M. Cheng, *Appl. Phys. Lett.* **2006**, *89*, 253112.
[32] K. Hou, C. Li, W. Lei, X. Zhang, K. Qu, X. Yang, Z. Zhao, B. Wang, K. Hou, C. Li, W. Lei, X. Zhang, K. Qu, X. Yang, Z. Zhao, B. Wang, *J. Vac. Sci. Technol., B* **2008**, *26*, 1305.
[33] F. Xu, K. Yu, G. Li, Q. Li, Z. Zhu, *Nanotechnology* **2006**, *17*, 2855.
[34] Q. F., L. X. F. L. Liao, J. C. Li, D. F. Wang, C. Liu, C. S. Liu, *Nanotechnology* **2005**, *16*, 985.
[35] C. Li, K. Hou, W. Lei, X. Zhang, B. Wang, X. W. Sun, *Appl. Phys. Lett.* **2007**, *91*, 163502.
[36] K. Hou, C. Li, W. Lei, X. Zhang, W. Gu, D. D. Engelsen, *Nanotechnology* **2007**, *18*, 335204.
[37] C. Florea, G. Brătucu, V. S. Păunescu, *Bull. Transilvania Univ. Brasov, Ser. II* **2012**, *5*, 147.
[38] D. I. Ozol, in *2014 Tenth Int. Vacuum Electron Sources Conf. (IVESC)* (Ed: N. V. Egorov), IEEE, Piscataway, NJ **2014**, pp. 1–2.
[39] M. Broxtermann, D. Den Engelsen, G. R. Fern, P. Harris, T. G. Ireland, T. Jüstel, J. Silver, *ECS J. Solid State Sci. Technol.* **2017**, *6*, R47.
[40] X. Wang, Y. Chen, F. Liu, Z. Pan, *Nat. Commun.* **2020**, *11*, 2040.
[41] R. H. Fowler, L. Nordheim, *Proc. R. Soc. London, Ser. A* **1928**, *119*, 173.
[42] C. X. Xu, X. W. Sun, *Appl. Phys. Lett.* **2003**, *83*, 3806.
[43] X.-P. Shen, A.-H. Yuan, Y.-M. Hu, Y. Jiang, Z. Xu, Z. Hu, *Nanotechnology* **2005**, *16*, 2039.
[44] Q. Wan, K. Yu, T. H. Wang, C. L. Lin, *Appl. Phys. Lett.* **2003**, *83*, 2253.
[45] N. Pan, H. Xue, M. Yu, X. Cui, X. Wang, J. G. Hou, J. Huang, S. Z. Deng, *Nanotechnology* **2010**, *21*, 225707.
[46] U. N. Maiti, S. Maiti, T. P. Majumder, K. K. Chattopadhyay, *Nanotechnology* **2011**, *22*, 505703.
[47] S. Maiti, U. N. Maiti, B. C. Behera, S. Pal, K. K. Chattopadhyay, *J. Mater. Chem. C* **2013**, *1*, 4940.
[48] N. S. Ramgir, I. S. Mulla, K. Vijayamohanan, D. J. Late, A. B. Bhise, M. A. More, D. S. Joag, *Appl. Phys. Lett.* **2006**, *88*, 042107.
[49] M. Kneissl, in *III-Nitride Ultraviolet Emitters: Technology and Applications* (Eds: M. Kneissl, J. Rass), Springer International Publishing, Cham **2016**, pp. 1–25.
[50] W. Kowalski, *Ultraviolet Germicidal Irradiation Handbook*, Springer Berlin Heidelberg, Berlin, Heidelberg, **2009**.
[51] C. S. Heilingloh, U. W. Aufderhorst, L. Schipper, U. Dittmer, O. Witzke, D. Yang, X. Zheng, K. Sutter, M. Trilling, M. Alt, E. Steinmann, A. Krawczyk, *Am. J. Infect. Control* **2020**, *48*, 1273.
[52] H. Inagaki, A. Saito, H. Sugiyama, T. Okabayashi, S. Fujimoto, *Emerging Microbes Infect.* **2020**, *9*, 1744.

© 2021 Wiley-VCH GmbH